Journal of Luminescence 235 (2021) 118012

Contents lists available at ScienceDirect

Journal of Luminescence

journal homepage: http://www.elsevier.com/locate/jlumin

Strong self-sensitized green and NIR emission in $NaYS_2$ doped with Pr^{3+} and Yb^{3+} by inducing Laporte allowed and charge transfer transitions

Per-Anders Hansen [a,*], Susmit Kumar [a], Andries Meijerink [b]

[a] Department of Chemistry, Centre for Materials Science and Nanotechnology, University of Oslo, Sem Sælandsvei 26, 0371, Oslo, Norway
[b] Debye Institute for NanoMaterials Science, Utrecht University, Utrecht, the Netherlands

ARTICLE INFO

Keywords:
Down conversion
Lanthanide
Sulphide
Solar cells
Sensitization

ABSTRACT

Down conversion of solar UV and blue light is one of the few ways of surpassing the Shockley-Queisser limit of solar cells. One of the most efficient down conversion systems is the Pr^{3+} - Yb^{3+} lanthanide pair. However, these ions do not provide any strong absorption for solar UV and blue light, thus require sensitizing. In this work, we report self-sensitization by inducing strong Laporte allowed f → d and charge transfer transitions on Pr^{3+} and Yb^{3+}, respectively. By replacing oxygen or fluorine anions with the more polarizable and reducible S^{2-}, the chemical bonds become more covalent, the d-shell of Pr^{3+} and the anion-to-Yb^{3+} charge transfer states are lowered into the near-UV and blue range. This avoids the need for a third strongly absorbing specie that may be difficult to include into the matrix or might provide other quenching routes by, for example, introducing new defects. The down conversion system can thus be kept simple, without more dopants types than the two lanthanides. The straightforward two-step synthesis of $NaYS_2$ is realized without toxic H_2S, and both precursor chemicals and produced material can be handled in air. The optical and chemical properties of $NaYS_2$, no need for an additional sensitizer and easy synthesis are strong arguments that the little explored $NaYS_2$-type materials deserves more attention.

1. Introduction

The use of solar cells is growing exceptionally fast, today providing about 3% of the world's electricity needs with crystalline silicon cells being the dominant technology (>95%) [1]. At the same time, silicon solar cells are rapidly approaching their theoretical limit of about 30%, the Shockley-Queisser limit [2]. In spring 2017, the record efficiency of a wafer sized silicon cell was 26.6% [3]. To continue this increase in efficiency, some technology that can surpass the Shockley-Queisser must be included while still being compatible with silicon. Down conversion is one such technology [4,5], which has the benefit of being very simple to include in panel designs compared to multi-junction approaches, as there is no need for direct electrical contact with the solar cell material.

Down conversion with close to 200% efficiency was demonstrated in fluoride materials in 1999 [6]. Silicon cells require that the emitted photons lie in the 900–1050 nm range while the absorption must lie in the 300–500 nm range. A large portion of down conversion materials is based on Yb^{3+}, which do emit in this range at 1000 nm. In particular, combining Yb^{3+} with Ce^{3+}, Pr^{3+} and Tb^{3+} have been investigated and shown promising results. The Ce^{3+}-Yb^{3+} couple is unfortunately shown to not facilitate down conversion [7]. The cooperative energy transfer from 1 Tb^{3+} to 2 Yb^{3+} is a very slow process, requiring very high Yb^{3+} concentrations which results in strong concentration quenching [8]. There are ways to reduce concentration quenching effects through nanostructuring [9,10] though. The stepwise energy transfer from Pr^{3+} to Yb^{3+} however is much more efficient [11]. For both Tb^{3+} and Pr^{3+}, sensitization in the UV/blue range is needed due to very weak intra-configurational 4f-4f absorption from these lanthanides.

Sensitization of these two ions in inorganic materials is not trivial as they are quenched by d^0 transition metals like in TiO_2 [12,13]. Tb^{3+} has been sensitized by organic species and Ce^{3+}, but this is difficult for Pr^{3+} as this ion is quenched by the high phonon energies in organic species and lack of overlap between Ce^{3+} emission and Pr^{3+} absorption. In addition, cooperative energy transfer from strongly absorbing species such as YVO_4 [14,15] and Bi^{3+} to Yb^{3+} have been attempted [16], but these also show slow and usually incomplete energy transfer even at high Yb^{3+} concentration where concentration quenching of Yb^{3+} lowers the overall quantum efficiency. A strongly sensitized Pr^{3+}-Yb^{3+} couple could be ideal for solar down conversion, yet it is still very hard to achieve.

* Corresponding author.
E-mail address: p.a.hansen@kjemi.uio.no (P.-A. Hansen).

https://doi.org/10.1016/j.jlumin.2021.118012
Received 23 October 2020; Received in revised form 17 February 2021; Accepted 23 February 2021
Available online 25 February 2021

In this work, rather than sensitizing Pr^{3+} and Yb^{3+} by other species, we induce strongly absorbing f → d (d^1) and charge transfer (CT) transitions on these ions with the more covalently bonded sulphur in the $ALnS_2$ family (A = Li, Na, K, Rb) [17–19], $NaYS_2$ in our case. Sulphide hosts allow strong and efficient sensitization while avoiding the synthesis complications and possible quenching mechanisms introduced by a third cation or other species [20]. The $ALnS_2$ family is a low-phonon host [21] and contains M^{3+} lanthanide sites, making it very well suited for sensitized lanthanide luminescence and in particular sensitized up conversion [22] and down conversion. The absorption and transfer mechanisms that are most important in this sensitized down conversion process is illustrated in Fig. 1. The strong and broad absorptions from the $NaYS_2$ host, Pr^{3+} f → d and Yb^{3+} CT transitions are marked with grey boxes while f levels of Pr^{3+} and Yb^{3+} are shown as horizontal bars. Possible energy transfer mechanisms are shown with arrows and numbered to be discussed in the discussion section.

Magnetic fields and induced magnetic flux in materials can influence the materials optical and luminescence properties [23], although the exact mechanisms and practical consequences varies to a large degree [24] and can be difficult to predict. Likewise, in-situ optical characterization during magnetic field experiments can provide valuable information for interpreting the results [25]. In addition, reports on the effect of magnetic fields on sulfide materials are rare. Therefore, we also investigate the effect that an increasing magnetic field up to 9 T (T) has on the luminescence properties of Pr^{3+} and Yb^{3+} in $NaYS_2$ at 300 K and 5 K. The temperature dependence of the luminescence is also reported.

2. Experimental

$NaYS_2$ powders doped with Pr^{3+} and/or Yb^{3+} were synthesized by a two-step process. First, a precursor powder was made by aqueous precipitation followed by firing a precursor powder at 1000 °C for 2 h in flowing nitrogen and CS_2. To make the precursor powders, lanthanide trichlorides were first dissolved in the desired ratios in water in one beaker and 10% excess over the stoichometric amount of Na_2S in water in another beaker. The content of these two beakers were then mixed under stirring, forming a white precipitate. The solvent was evaporated using an electric heating plate, leaving a white cake. This cake was then dried at 130 °C in an oven in air over night, resulting a brittle white mass that was crushed to a fine powder with an agate mortar. This powder showed no sign of crystallinity in XRD. The powder was put in alumina crucibles and fired for 2 h in a tube furnace at 1000 °C in flowing CS_2 containing nitrogen. CS_2 was introduced by bubbling the nitrogen through liquid CS_2 cooled in an ice bath. The tube furnace was flushed with this gas mixture for 1 h before heating at 5 °C/min. The overall reaction is given below, exemplified with only yttrium. Although CS_2 does not seem necessary in this reaction, some crystal water is likely present in the fired powder as oxide phases was formed when fired in only nitrogen. The produced NaCl sublimes at 1000 °C and is carried downstream by the flowing nitrogen.

$$2Na_2S + YCl_3 \rightarrow NaYS_2 + 3\,NaCl$$

Several types of samples were produced. These are undoped $NaYS_2$, single doped $NaYS_2$: 1% Pr^{3+} and $NaYS_2$: 1% Yb^{3+}, and double doped $NaYS_2$: 1% Pr^{3+}, x% Yb^{3+} where x = 0–25%. Dopant lanthanides replace an equal amount of yttrium. For easier reference in this text, these are named $NaYS_2$, $NaYS_2$:Pr, $NaYS_2$:Yb and xYb, respectively. The 0 Yb sample (x = 0) correspond to $NaYS_2$:Pr.

Luminescence (PL) and excitation (PLE) measurements were done using an Edinburgh Instruments FLS920 fluorescence spectrometer with a 450 W Xe lamp as excitation source, and a Hamamatsu R928 PMT and a liquid-nitrogen cooled Hamamatsu R5509-42 PMT for detection in the UV–Vis and NIR range, respectively. PL decay measurements were performed with an optical parametric oscillator (OPO) system (Opotek HE 355 II) pumped by the third harmonic of a Nd:YAG laser as excitation source. The OPO system was set to 355 nm and a repetition rate of 20 Hz. The decay was recorded with the same equipment used for the excitation measurement.

PL with and without applied magnetic field in the 300–5 K temperature range was done in a Quantum Design Physical Property Measurement System (QD-PPMS), using a 280 nm UV diode as excitation source, and USB4000 and NIRQuest spectrometers (OceanOptics) for detection of visible and NIR emissions. The PPMS operated under vacuum. The powder samples were held in thin perforated gelatin capsules that allowed evacuation of the capsule interior without breaking. The capsule was then mounted on a long silica rod that acted as waveguide for excitation and emission light through an O-ring seal to avoid breaking the vacuum. The samples were mounted in close proximity to the system thermometer, utilizing platinum and CERNOX® thermocouples for accurate temperature read-out. Samples were left for 30 min at 5 K to thermally homogenize before starting magnetic field dependent measurements.

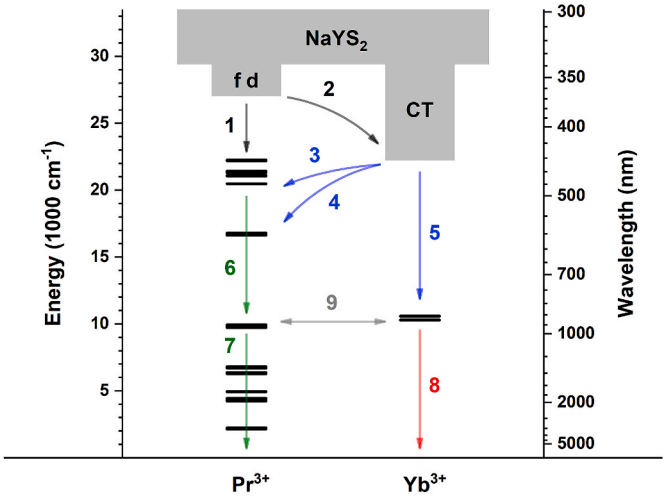

Fig. 1. Energy level diagram of Pr^{3+} and Yb^{3+} doped $NaYS_2$ showing absorption in the $NaYS_2$ host itself, f levels (horizontal lines, from $LaCl_3$ [26]), d^1 level of Pr^{3+}, CT level of Yb^{3+} and a selection of the many possible energy transfers in this system.

3. Results

3.1. Synthesis

Fig. 2 shows the X-ray diffractogram (XRD) of an undoped sample, showing phase pure $NaYS_2$. It is clear that the produced powder does not contain any NaCl. NaCl has a vapour pressure of about 1.2 kPa at 1000 °C and was carried away by the flowing atmosphere. A white condensate consisting of NaCl was found downstream in the furnace tube. Firing at 900 °C did not provide a high enough vapour pressure of NaCl and at this temperature it was found also in the produced powder sample. Thus, firing at 1000 °C in a flowing atmosphere is a convenient way of removing the co-produced solid NaCl in-situ during synthesis. However, a small amount of black material was found in and around the alumina boat, indicating some carbon formation. Some of this was inevitably included in the sample powders. The amount of this black material was too small to characterize by XRD and is assumed to be carbon from the CS_2.

3.2. Luminescence

Fig. 3-**a** and **b** shows the emission spectra of $NaYS_2$:Pr, $NaYS_2$:Yb and 0.2 Yb, while their excitation spectra are shown in **c**. These samples show the different excitation and emission spectra of Pr^{3+} and Yb^{3+}. In addition, the spectra arising from combining the two ions in 0.2 Yb 0.2

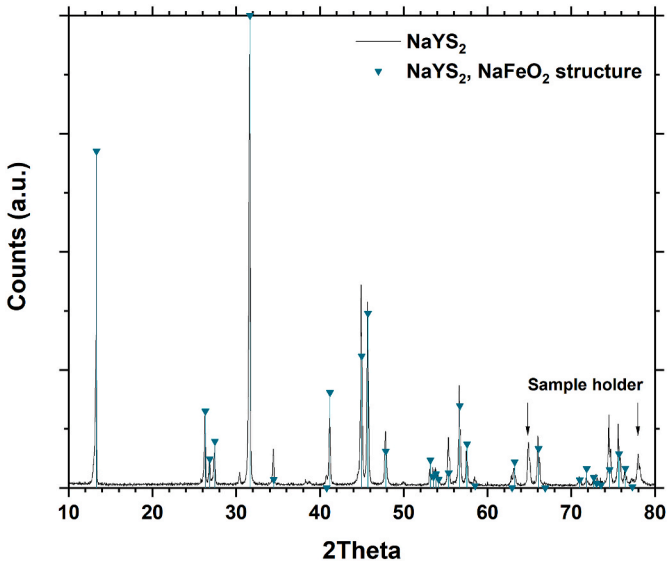

Fig. 2. XRD spectrum and diffraction pattern of $NaYS_2$.

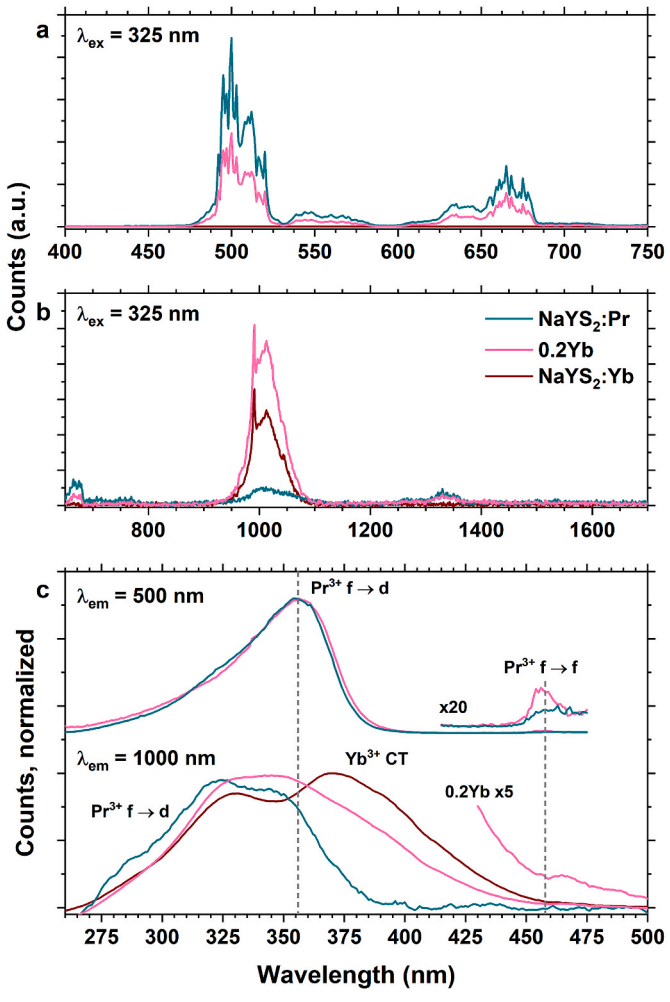

Fig. 3. Overview of emission and excitation profiles of Pr^{3+} and Yb^{3+} in addition to their combination in $NaYS_2$:Pr, $NaYS_2$:Yb and 0.2 Yb a visible emission, b NIR emission, c excitation of Vis and NIR emissions. Note the differences in wavelengths (x-axis).

Yb is chosen as it has the strongest emission in both Vis and NIR among the xYb samples. For the visible emission, $NaYS_2$:Pr shows the strongest emission, while $NaYS_2$:Yb shows no emission in this range. 0.2 Yb shows a reduced Vis emission compared to $NaYS_2$:Pr. All the three samples show NIR emissions. $NaYS_2$:Pr shows emissions at both 1000 and about 1350 nm $NaYS_2$:Yb shows only emission at 1000 nm. The Pr^{3+} and Yb^{3+} emissions at 1000 nm overlap almost exactly, but the Yb^{3+} emission can be distinguished by the sharp peak at 980 nm. 0.2 Yb shows both the 980 nm peak of Yb^{3+} and 1350 nm emission of Pr^{3+}. Interestingly, 0.2 Yb shows a stronger 1000 nm emission than both the single doped samples.

In the PLE spectra (Fig. 3-**c**), the 500 nm emissions of $NaYS_2$:Pr and 0.2 Yb show identical profiles indicating that the excitation processes resulting in Pr^{3+} $^3P_0$-emission is the same in both single doped and double doped samples with no additional component from the Yb^{3+} CT absorption. The excitation profile is dominated by the Laporte allowed f → d transition on Pr^{3+} at 355 nm, but the much weaker f → f transitions are also visible at 455 nm ($^3H_4$–$^3P_2$). The intensity of the f → d transition is about 180 stronger than the f → f transitions. The excitation spectra of the 1000 nm emissions show more variation. The 500 and 1000 nm emissions of $NaYS_2$:Pr show different spectra, although in the same 275–375 nm range. Thus, it seems like excitation process for Pr^{3+}'s 1000 nm emission is not the same as for the 500 nm emission. Yb^{3+} show two dominant broad peaks that span longer wavelengths towards 450 nm. The 0.2 Yb sample show a spectrum containing features of both. The different types of transitions are marked in the figure. The f → f transitions are not visible for $NaYS_2$:Pr's 1000 nm emission, possibly because the overall emission intensity at this wavelength is quite low. For 0.2 Yb, this emission is much stronger and observation of these transitions could be expected. One weak feature is visible at about 465 nm, but it is overlapping with the Yb^{3+} CT transition. As the absorption due to the CT transition is very strong, it is likely that the f → f transitions are obscured.

Optical absorbance spectra of the $NaYS_2$ host, singly doped $NaYS_2$:Pr and $NaYS_2$:Yb is shown in Fig. 4-**a**, in addition to the xYb series with increasing Yb content in **b**. $NaYS_2$ itself has two strong absorption peaks

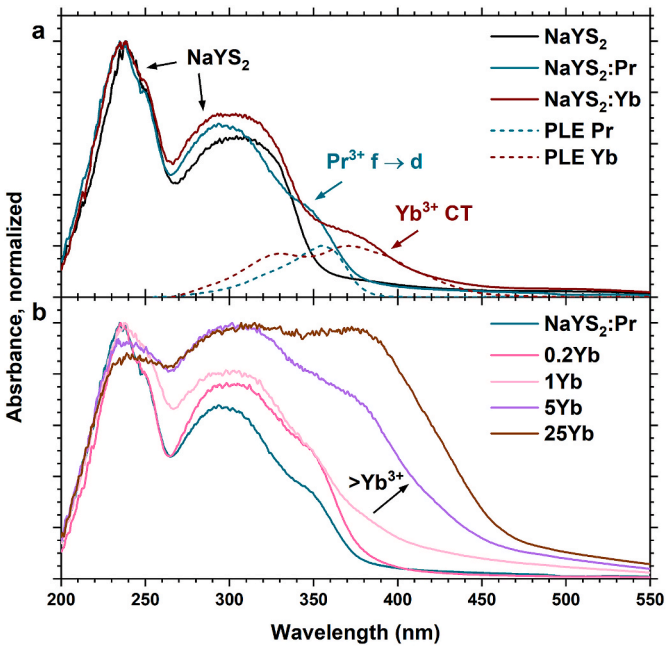

Fig. 4. Normalized absorption spectra of $NaYS_2$, $NaYS_2$:Pr and $NaYS_2$:Yb highlighting the absorption of the $NaYS_2$ matrix, Pr^{3+} f → d and Yb^{3+} CT transitions (a), and xYb samples (b). Dotted lines are normalized PLE of 500 nm emission for $NaYS_2$:Pr and 1000 nm emission from $NaYS_2$:Yb. Note that $NaYS_2$:Pr and 0 Yb is the same sample.

centred around 240 and 307 nm, with an absorption tail extending to about 350 nm $NaYS_2$:Pr shows an additional shoulder at about 350 nm with a tail until 370 nm which can be assigned to the Pr^{3+} f → d transition, while the shoulder for $NaYS_2$:Yb is identified as Yb^{3+} CT transition at about 380 nm with a tail until 450 nm. PLE of 500 nm and 1000 nm emissions from $NaYS_2$:Pr and $NaYS_2$:Yb are shown in dotted lines and correspond very well to the two additional absorption shoulders.

For the 1% single doped samples, the Pr^{3+} f → d and Yb^{3+} CT transitions have similar absorption strength. Fig. 4-b shows the evolution of the absorption of $NaYS_2$:Pr upon adding 0.2, 1, 5 and 25% Yb^{3+}. Upon 5% and more doping, the absorption from Yb^{3+} CT is stronger than that of the $NaYS_2$ host.

Fig. 5 shows the PLE spectra of 500 nm (**a**) and 1000 nm (**b**) emission of the single doped and xYb samples. The 500 nm emission decreases rapidly even for small concentrations of Yb^{3+} and is more or less fully quenched for Yb-concentrations >1%. The addition of Yb^{3+} does not change the spectrum shape, indicating that there is no Yb^{3+} CT → Pr^{3+} energy transfer. The 1000 nm emission on the other hand benefits from co-doping with both Pr^{3+} and Yb^{3+}. $NaYS_2$:Pr show a relatively weak 1000 nm emission compared to $NaYS_2$:Yb, which is expected. The 1000 nm $^2F_{5/2}$-$^2F_{7/2}$ emission of Yb^{3+} is the only possible emission from the $^2F_{5/2}$ level of Yb^{3+}. The 1000 nm $^1G_4$-$^4H_4$ emission of Pr^{3+} has a low oscillator strength and competing $^1G_4$ emissions occur to other 4f levels (e.g. 1350 nm emission). The 1 Yb and in particular 0.2 Yb show stronger 1000 nm emission than either of the single doped samples. The PLE spectra also changes with changing Yb concentration where 0.2 Yb show a spectrum that is a superposition of $NaYS_2$:Pr and $NaYS_2$:Yb while 1 Yb and higher concentrations has mostly $NaYS_2$:Yb character.

Fig. 6 shows decay curves for the 500 nm (**a**) and 1000 (**b**) emissions of $NaYS_2$:Pr, $NaYS_2$:Yb and selected xYb samples. The 1000 nm emission decays can be modelled with a single exponential function, while the 500 nm emission show more components. The single exponential lifetime of 1000 nm and mean lifetime (when $I = I_0/\pi$) of 500 nm emissions are plotted in Fig. 7-**b**.

Fig. 7-**a** shows the 500 and 1000 nm emission intensities as a function of Yb^{3+} concentration upon excitation at 355 nm (Pr^{3+} f → d) and 375 nm (Yb^{3+} CT), respectively, while Fig. 7-**b** show these emissions lifetimes. Single doped $NaYS_2$:Yb is shown on the left, while 0 Yb represents single doped $NaYS_2$:Pr. The decrease in intensity of 500 nm is

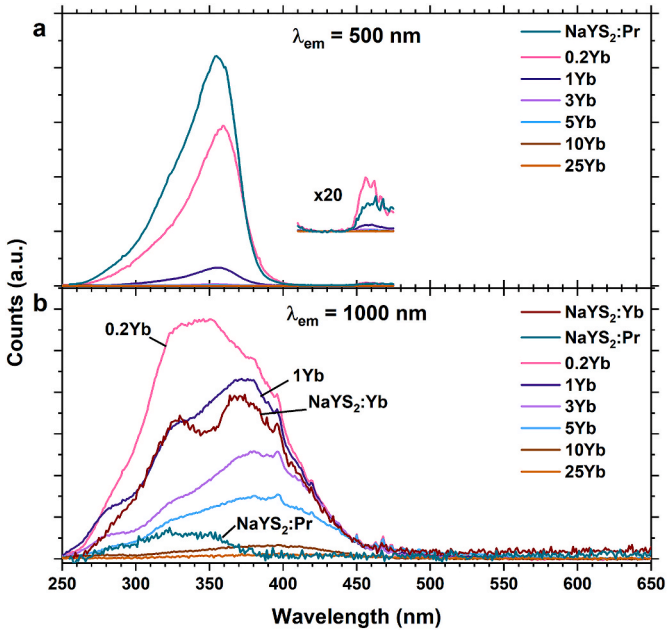

Fig. 5. PLE spectra the 500 nm (a) and 1000 nm (b) emission of $NaYS_2$:Pr, $NaYS_2$:Yb and xYb samples.

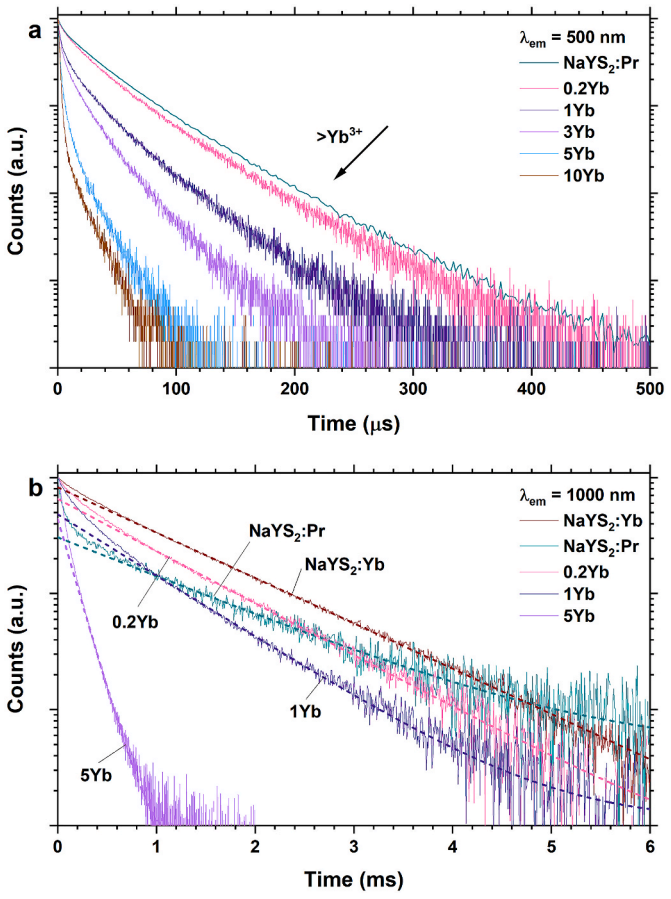

Fig. 6. Decay curves for the 500 nm (λ_{ex} = 457 nm, a) and 1000 nm (λ_{ex} = 355 nm, b) emissions of $NaYS_2$:Pr, $NaYS_2$:Yb and selected xYb samples. The 1000 nm is modelled with a single exponential function, shown with dashed lines.

much stronger than for 1000 nm with increasing Yb concentration and a similar decrease is seen in the lifetimes. One possibility for the decrease in 500 nm emission intensity is shadowing from the strong Yb^{3+} CT absorption that overlaps with the Pr^{3+} f → d absorption, effectively decreasing the amount of excitation light absorbed by Pr^{3+}. However, the decrease in lifetime shows that quenching of the $^3P_0$ state is the major cause, likely due to cross relaxation with Yb^{3+}. The 1000 nm emission intensity is higher for both 0.2 Yb and 1 Yb compared to $NaYS_2$:Yb (data point at the very left in the figure) even though the lifetime is shorter. This indicates that the presence of Pr^{3+} aids the overall energy transfer pathways from excited f → d or CT states down to the excited Yb^{3+} $^2F_{7/2}$ state.

3.3. *Influence by temperature and magnetic field*

Temperature and magnetic fields can have a large effect on emission, transfer and quenching processes, and can provide a path to tune and improve the materials optical properties. The Vis and NIR spectra were measured while cooling to cryogenic temperatures (5 K), while the magnetic field was changed from 0 to 9 to 0 T at 300 and 5 K. These measurements were conducted for $NaYS_2$:Pr, $NaYS_2$:Yb and 0.2 Yb. Integrated intensities of 500 nm and 1000 nm intensities are integrated in the 450–530 nm 950–1150 nm range.

The integrated 500 nm and 1000 nm emissions from $NaYS_2$:Pr and $NaYS_2$:Yb as a function of temperature is shown in Fig. 8. The NIR emission of $NaYS_2$:Pr was too weak to be detected in this setup. The 500 nm emission is seen to have a maximum at around 150 K, indicating some level of quenching at room temperature, while is has a stable value below 50 K. The 1000 nm emission show less temperature dependence.

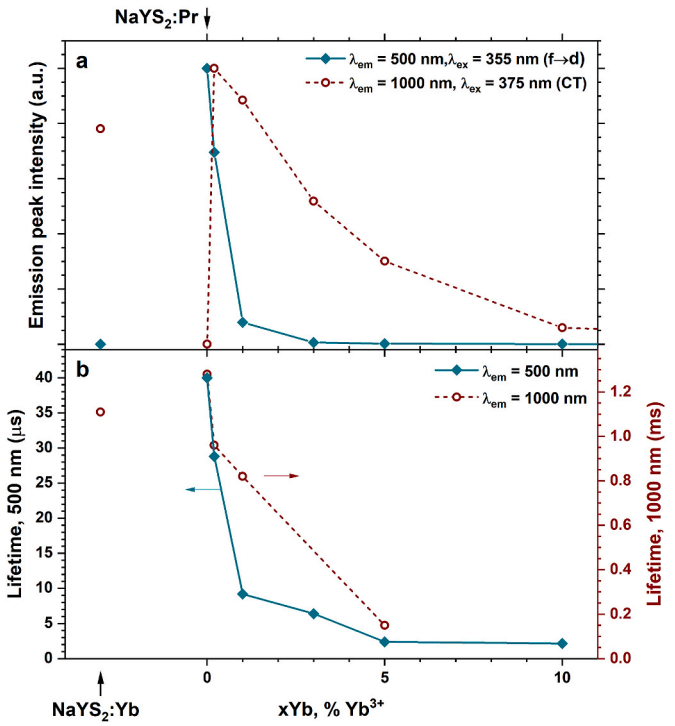

Fig. 7. Emission peak intensities (a) and lifetimes (b) of $NaYS_2$:Pr, $NaYS_2$:Yb and xYb samples. $NaYS_2$:Yb is shown on the left while xYb follows the x-axis units with $NaYS_2$:Pr as 0 Yb. The lifetimes of 500 nm emissions are the mean lifetime, i.e. when $I = I_0/\pi$, while the 1000 nm emissions is the single exponential lifetime.

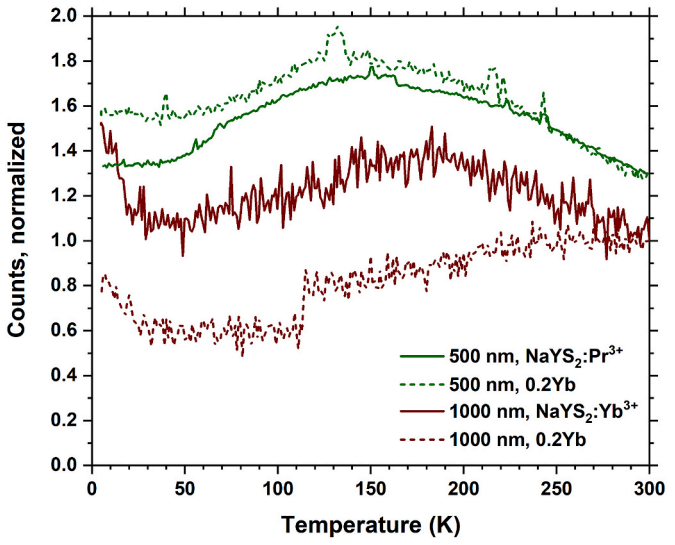

Fig. 8. The integrated emissions of $NaYS_2$:Pr, $NaYS_2$:Yb and 0.2 Yb as a function of temperature, $\lambda_{ex} = 280$ nm. The 500 nm counts were integrated over 450–530 nm, while the 1000 nm counts were integrated over 950–1150 nm. Green and dark red colors are used to indicate green (500 nm) and NIR (1000 nm) emissions.

The emission spectra experienced a gradual change at low temperatures, starting at about 150 K for 500 nm and about 180 K for 1000 nm. The emission spectra at 300 and 5 K is shown in Fig. 9. The Vis spectra are identical for $NaYS_2$:Pr and 0.2 Yb, and so is the NIR spectra of $NaYS_2$:Yb and 0.2 Yb. Thus, only the Vis spectra of $NaYS_2$:Pr and NIR spectra of $NaYS_2$:Yb is shown.

PL as a function of magnetic field is not often conducted, and we have

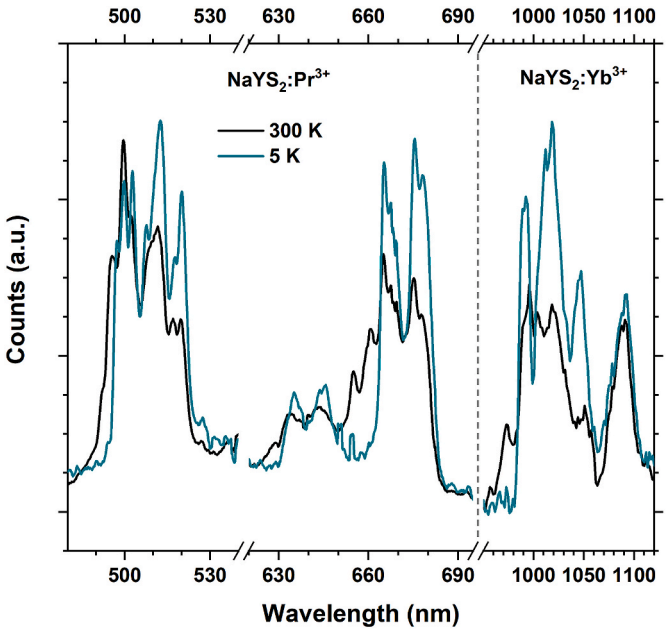

Fig. 9. The Vis emission spectra of $NaYS_2$:Pr and NIR emission spectra of $NaYS_2$:Yb at 300 and 5 K, showing the change in spectrum shape for single doped samples. The double doped 0.2 Yb sample showed identical emission spectrum and spectrum changes in the Vis and NIR range as the single doped $NaYS_2$:Pr and $NaYS_2$:Yb samples.

not found any reports of the luminescence properties of $ALnS_2$ material class in magnetic fields. We found that both the intensities and spectra shapes of Vis and NIR emissions of $NaYS_2$:Pr and $NaYS_2$:Yb we unaffected by magnetic fields up to 9 T both at 300 and 5 K.

4. Discussion

4.1. Synthesis chemical stability

All the synthesis steps, characterizations and storage are done in air with no measures to protect the sample from oxygen or moisture. The only exception is the firing step with CS_2 flow which is done in a nitrogen atmosphere. The samples show no visible degradation after being exposed to air for more than one year indicating that $NaYS_2$ is a quite air stable material. This makes sample handling and synthesis more practical than for more air sensitive sulphide materials.

The XRD in Fig. 2 show that this synthesis route produce phase pure $NaYS_2$, with no crystalline contamination. This means that the NaCl by-product is effectively removed by the gas flow at 1000 °C. NaCl deposits were found downstream in the oven tube. Firing at 900 °C was found to be insufficient to evaporate NaCl and large amounts was found in addition to $NaYS_2$ in XRD. However, 1000 °C is not necessary for the formation of $NaYS_2$ as it was also formed with no other sulphur or lanthanide phases detected by XRD at 900 °C as long as nitrogen containing CS_2 was used. Without CS_2, other peaks appeared in the XRD data which we could not identify but likely comes from oxide phases formed by a reaction with crystal water.

Thus, to obtain oxide-free $NaYS_2$ it was necessary to use a stream of CS_2. It is likely that this reaction can be carried out at lower temperatures than 900 °C as well. To also obtain NaCl-free powder, the powder should be heated to 1000 °C under flowing nitrogen to evaporate and remove the NaCl. CS_2 is likely not necessary in this step although evaporation of NaCl without CS_2 was not attempted in this work. Another possible way of removing NaCl is by washing with water after the firing step. It was attempted to remove NaCl by grinding the sample powder and stirring it with DI water. The $NaYS_2$ did not seem to deteriorate by this treatment, but it was also found insufficient to remove all

NaCl. Thus, it was decided that evaporation at 1000 °C was more practical in this work, although this also led to some carbon formation.

For future work based on this synthesis route, it would be beneficial to do the CS_2 firing step to form $NaYS_2$ at lower temperatures to avoid decomposition of CS_2 and carbon formation (as this was not seen at 900 °C), then continue the firing at 1000 °C in pure nitrogen to evaporate NaCl.

4.2. Optical properties

It is useful to compare the materials in this work, with previously developed down conversion materials based on Pr^{3+} and Yb^{3+} doped YF_3 [27]. In YF_3, down conversion was proven by careful comparison of excitation processes leading to 1000 nm emission. However, YF_3:Pr^{3+}, Yb^{3+} provides no strong absorption mechanisms in the solar UV or blue range. The main goal in the current work was to introduce strong absorption mechanisms without introducing other metal species like Ce^{3+}. Thus, replacing fluorine with sulphur was chosen. Compared to YF_3:Pr^{3+},Yb^{3+}, $NaYS_2$:Pr^{3+},Yb^{3+} has three different and strong absorption mechanisms; the $NaYS_2$ host itself, f → d transitions on Pr^{3+} and CT transitions on Yb^{3+}. These are all strong and broad absorption, with large overlaps. This is very beneficial as it allows strongly sensitized down conversion of solar light to be realized. It also makes the interpretation of the optical data more complicated as $NaYS_2$:Pr^{3+},Yb^{3+} contains different types of overlapping absorption and new possible energy transfer routes compared to the simpler YF_3:Pr^{3+},Yb^{3+}. Thus, this discussion will be divided in more detailed discussions about the absorption and excitation, and emission and possible down conversion processes.

4.2.1. Absorption and excitation processes

The absorption of undoped, single-doped and co-doped $NaYS_2$ is shown in Fig. 4-**a**, along with PLE spectra for 500 nm emission in $NaYS_2$:Pr and 1000 nm emission for $NaYS_2$:Yb. The Pr^{3+} f → d and Yb^{3+} CT transitions can be seen as shoulders on the long wavelength side of the host $NaYS_2$ absorption. The two PLE spectra correspond very well with these two absorption shoulders. However, the PLE spectra also illustrate the shadowing effect of the higher energy absorptions, i.e. parasitic absorption by $NaYS_2$ lowers the PLE of Pr^{3+} 500 nm emission at the short wavelength side of the emission peak.

Comparing Figs. 3 and 4, it is apparent that absorption through the $NaYS_2$ host itself does not lead to emission in either Pr^{3+} nor Yb^{3+}. Thus, this absorption mechanism is ineffective as a sensitizer in this down conversion system and only provides parasitic absorption. The absorption through Pr^{3+} f → d transitions on the other hand leads to strong visible and weak NIR emission in $NaYS_2$:Pr. This sample also show strong green luminescence under a UV lamp. The weaker f-f transitions on Pr^{3+} can be seen around 455 nm. Looking at the 1000 nm emission PLE in Fig. 5, it is seen that the 1000 nm emission of 0.2 Yb has character of both the single doped samples, i.e. $NaYS_2$:Pr and $NaYS_2$:Yb. Thus, it can be concluded that absorption through the Pr^{3+} f → d transition is followed by energy transfer to the $^3P_0$ states of Pr^{3+} and possibly also to the Yb^{3+} CT state. However, when looking at the 500 nm emission PLE in the same figure, no sample show any character of the $NaYS_2$:Yb^{3+} samples 1000 nm emission nor any strong lower energy excitation than the Pr^{3+} f → d transition apart from the much weaker Pr^{3+} f → f transitions. In fact, all the emissions in the visible 400–700 nm range show identical shape of their PLE spectra, i.e. there is no energy transfer from the Yb^{3+} CT state to neither Pr^{3+}'s $^3P_0$ nor $^1D_2$ states. Only the 1000 nm emission has distinctly different PLE spectra. Thus, it seems that the only energy transfer from the Yb^{3+} CT state is to the lower $^2F_{7/2}$ Yb^{3+} excited state.

4.2.2. Down conversion and emission

Using S^{2-} as anions for the Pr^{3+}/Yb^{3+} down conversion couple introduces strong and broad absorption bands in the near-UV and blue range, which effectively sensitize the visible and NIR emission of both Pr^{3+} and Yb^{3+}. It is clear from Figs. 4 and 5 that both the Pr^{3+} f → d transition and Yb^{3+} CT transition leads to 1000 nm emission. However, it is not straight forward to explain how the energy is transferred from these two absorbing states to the emitting state of Yb^{3+}. For the YF_3:Pr^{3+},Yb^{3+} case, down conversion can be proven with the PLE spectra of the 1000 nm emission and carefully comparing the intensity of the $^3P_0$ and $^1D_2$ peaks. However, this is not possible in the $NaYS_2$:Pr^{3+}, Yb^{3+} case, as Yb^{3+} CT absorption tail overlaps with the $^3P_0$ excitation.

The down conversion process in Pr^{3+}/Yb^{3+} pairs is a two-step process, starting from the green emitting $^3P_0$ state of Pr^{3+}. The first step consists of this state relaxing to the lower $^1G_4$ state, exciting one neighbouring Yb^{3+} in the process. The next step is relaxation from the $^1G_4$ to the $^3H_4$ ground state, exciting another Yb^{3+}. These two steps are illustrated as arrow 6 and 7 in Fig. 1. This process will effectively split a single high energy excited state into two lower energy excited states, given that both steps work efficiently. If one these two steps are inefficient, it is still possible to obtain strong 1000 nm Yb^{3+} emission, though the efficiency cannot reach 200%. For efficient down conversion, both steps must be efficient. One way to verify if both steps are efficient is to carefully compare the 1000 nm emission upon $^3P_0$ and $^1D_2$ excitation. If the experimental setup is properly calibrated and excitation through $^3P_0$ gives twice the amount of 1000 nm luminescence compared to excitation through $^1D_2$, this means that the $^3P_0$ indeed produces two photons. This is the case in YF_3. Unfortunately, it is not possible to do this in $NaYS_2$, as the Yb^{3+} CT absorption overlaps with the $^3P_0$ level, reducing the apparent luminescence yield from $^3P_0$. It can be seen from Fig. 7 that the $^3P_0$ state is strongly quenched by increasing Yb^{3+} content, meaning that there is effective non-radiative energy transfer from this state to Yb^{3+}. However, it is at this point uncertain through which process(es) the energy is transferred.

The Yb^{3+} CT state produces strong Yb^{3+} 1000 nm emission in $NaYS_2$:Yb. On the other hand, the CT state does not lead to visible emission from Pr^{3+}. As both $^3P_0$ and $^1D_2$ are emissive in 0.2 Yb and 1 Yb, but only show Pr^{3+} character in their PLE spectra, it can be concluded that the transfers from Yb^{3+} CT to these (illustrated by arrow 3 and 4 in Fig. 1) is not present, while CT → $^2F_{5/2}$ (arrow 5) is efficient. The Yb^{3+} CT state thus cannot produce down conversion in $NaYS_2$.

4.2.3. Summary of energy transfers

When Pr^{3+} and Yb^{3+} is doped into $NaYS_2$ compared to YF_3, the two additional f-d and CT states makes the possible energy transfers in the system a lot more complicated. Fig. 1 gives and overview of possible energy transfer mechanisms that relates directly to the desired stepwise down conversion process in Pr–Yb pairs. Here, we summarize which processes that have been confirmed to be present or not in this work.

Starting from the highest energies, there is no energy transfer from the $NaYS_2$ absorption bands to neither Pr^{3+} nor Yb^{3+}. The Pr^{3+} f-d state sensitizes the Pr^{3+} $^3P_0$ state **(1)**, but whether it also transfers energy to the lower lying Yb^{3+} CT state **(2)** is uncertain. The Yb^{3+} CT does not sensitize neither the $^3P_0$ **(3)** nor the $^1D_2$ **(4)** states of Pr^{3+}, but do sensitize the Yb^{3+} $^2F_{5/2}$ state **(5)**. As the Pr^{3+} $^3P_0$ state is central to the down conversion mechanism, **(3)** is one of the most important transfer in $NaYS_2$:Pr, Yb as it controls whether the Yb^{3+} CT state contributes positively or negatively to down conversion. From the Pr^{3+} $^3P_0$ state, both **(6)** and **(7)** may be possible. Pr^{3+} emits at 1000 nm, so either one or both should occur. The Pr^{3+} f-d state certainly sensitizes the Yb^{3+} emission, but this may happen either through **(1)**+**(6)** or **(2)**+**(5)**, or another route. (8) definitely occurs as it is responsible for the Yb^{3+} 1000 nm emission, while (9) is uncertain. In conclusion, f-d sensitization of down conversion may occur, but this cannot be determined by comparing PLE spectra in $NaYS_2$ as it is done for YF_3. The CT state does not sensitize down conversion.

4.3. Solar spectrum

Pr^{3+} and Yb^{3+} in $NaYS_2$ give rise to strong near-UV and blue absorption that can be used in solar energy harvesting. Both are broad and allowed transitions, making this an efficient sensitizing system. The $NaYS_2$ host has an absorption itself as well, which can cause parasitic absorption of solar UV. Fig. 10 show the part of the solar AM1.5 spectrum that can be utilized by silicon solar cells. The grey, blue and red areas indicate how much of this spectrum the $NaYS_2$, Pr^{3+} f → d and Yb^{3+} CT transitions absorb individually, i.e. if it was the only absorption process. It shows that even though $NaYS_2$ does indeed block some solar UV, this is only 0.6% of the photons that are useable by silicon solar cells. The Pr^{3+} and Yb^{3+} absorptions on the other hand can absorb 1.6 and 8.1% of these photons, respectively. Thus, the Yb^{3+} CT transition is particularly interesting for absorbing high energy sunlight.

4.4. Effects of temperature and magnetic field

Both the 500 nm emission of Pr^{3+} and 1000 nm emission of Yb^{3+} show an increase in emission with increasing temperature from 5 K to a maximum at about 150 K and 180 K for Vis and NIR emission, respectively. Further increase towards room temperature reduces emission intensity for both. This indicates both thermally activated emission, likely related to the transfer from the Pr^{3+} d^1 and Yb^{3+} CT states to the respective lanthanides f-manifold, and increasing quenching even at room temperature.

Influencing luminescence properties with magnetic fields is known, with several example of both sensitized luminescence and more advanced forms like upconversion given in a recent review and references therein [23]. It is clear from literature though that the practical effect on a sample by an applied magnetic field is not so straight forward to predict. Both absorption and emission can be affected, and the overall effect can be both negative and positive [24]. The effect is more often a decrease in overall emission intensity, although this is not negative by itself as it can allow optical measurement of local magnetic fields [28]. It is both time consuming and instrumentation wise difficult to obtain the necessary data to confirm which mechanisms that are important in strong magnetic fields.

The two single-doped samples in our work are unaffected by magnetic fields up to 9 T at both 300 and 5 K, leading to the conclusion that magnetic fields do not affect neither the absorption nor the transition probabilities in the range investigated here. Although the effect of magnetic fields were abent, the $ALnS_2$ material family allows substitutions with other magnetically active ions like Gd^{3+}. In fact, Du et al. showed that there was a decrease in Eu^{3+} emission intensity in YVO_4:Eu^{3+}, but an increase in $GdVO_4$:Eu^{3+} [24]. Thus, utilizing magnetization of the host material is an unexplored venue for affecting down conversion for example by introducing Gd^{3+} into the $ALnS_2$ host as a co-dopant or as pure $AGdS_2$.

5. Conclusion

In this work we have synthesized air-stable $NaYS_2$:Pr^{3+}, Yb^{3+} that show broad and strong near-UV and blue absorption coming from Pr^{3+} f → d and Yb^{3+} CT transitions in addition to strong 1000 nm emission, making this material very interesting for down conversion of high energy sunlight. Investigation of the possible down conversion process in this material show that Yb^{3+} CT transition results in strong 1000 nm emission and that this is a down shifting process, i.e. 1 UV to 1 NIR photon. The Pr^{3+} f → d transition on the other hand leads to a two-step energy transfer process to Yb^{3+} and possible down conversion. However, as the Yb^{3+} CT transition does not populate the Pr^{3+} $^3P_0$ state and it is the CT state that absorbs at lowest energies, this makes down conversion with Pr^{3+}/Yb^{3+} in $NaYS_2$ difficult. $NaYS_2$ belongs to a large family of similar $ALnS_2$ which will all give rise to both Pr^{3+} f → d and Yb^{3+} CT transition. With different A and Ln cations (Na, K, Rb/Y, La, Gd, Lu etc), it could be possible to decrease the Yb^{3+} CT → $^2F_{5/2}$ transfer rate and allow CT → $^3P_0$ transfer. This work is the first that introduces Yb^{3+} in the $ALnS_2$ family, so how this CT state and subsequent transfer processes change with different A and Ln cations is an unexplored area. This work is also the first to report on the effect of magnetic fields on optical and luminescence properties in the $ALnS_2$ material family. The possibility of replacing Ln partially or fully with Gd^{3+} might amplify the interactions with magnetic fields.

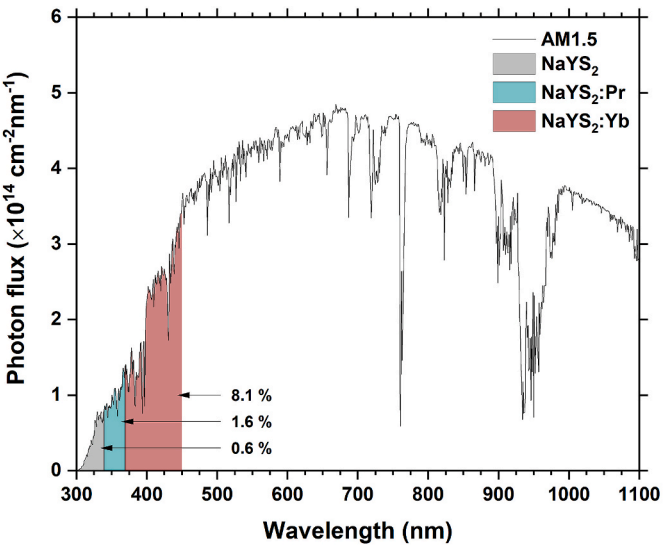

Fig. 10. Solar AM1.5 spectrum for shorter wavelengths than 1100 nm, i.e. what can be effectively used by silicon solar cells. The portion of this light that is absorbed by $NaYS_2$, Pr^{3+} in $NaYS_2$ and Yb^{3+} in $NaYS_2$ is marked with grey, blue and red respectively. The percentages represent the amount of energy in this 300–1100 nm spectrum that can be absorbed by each absorption mechanisms, assuming no shadowing effect from the other higher energy absorptions.

Credit statement

Per-Anders Hansen: Conceptualization, Methodology, Investigation, Writing – original draft, Visualization, Funding acquisition, Susmit Kumar: Methodology, Investigation, Writing – review & editing, Andries Meijerink: Resources, Writing – review & editing, Supervision.

Declaration of competing interest

The authors declare that they have no known competing financial interests or personal relationships that could have appeared to influence the work reported in this paper.

Acknowledgements

This work was performed within "The Norwegian Research Centre for Solar Cell Technology" project number 193829, a Centre for Environment-friendly Energy Research co-sponsored by the Research Council of Norway and research and industry partners in Norway.

References

[1] A. Jäger-Waldau, PV Status Report 2018, 2018.
[2] W. Shockley, H.J. Queisser, Detailed balance limit of efficiency of p-n junction solar cells, J. Appl. Phys. 32 (3) (1961) 510–519.
[3] K. Yoshikawa, et al., Silicon heterojunction solar cell with interdigitated back contacts for a photoconversion efficiency over 26%, Nature Energy 2 (2017) 17032, https://doi.org/10.1038/nenergy.2017.32.
[4] M.A. Green, S.P. Bremner, Energy conversion approaches and materials for high-efficiency photovoltaics, Nat. Mater. 16 (2016) 23, https://doi.org/10.1038/nmat4676.

[5] T. Trupke, M.A. Green, P. Wurfel, Improving solar cell efficiencies by down-conversion of high-energy photons, J. Appl. Phys. 92 (3) (2002) 1668–1674.
[6] R.T. Wegh, et al., *Visible quantum Cutting in $LiGdF_4:Eu^{3+}$ through downconversion*, Science 283 (5402) (1999) 663–666, https://doi.org/10.1126/science.283.5402.663.
[7] D.C. Yu, et al., *Insights into the energy transfer mechanism in $Ce^{3+}-Yb^{3+}$ codoped YAG phosphors*, Phys. Rev. B 90 (16) (2014) 165126.
[8] P. Vergeer, et al., *Quantum cutting by cooperative energy transfer in $Yb_xY_{1-x}PO_4:Tb^{3+}$*, Phys. Rev. B 71 (1) (2005), 014119.
[9] P.-A. Hansen, et al., Controlling luminescence and quenching mechanisms in subnanometer multilayer structure of europium titanium oxide thin films, J. Lumin. 215 (2019) 116618, https://doi.org/10.1016/j.jlumin.2019.116618.
[10] P.-A. Hansen, et al., *Luminescent Properties of multilayered Eu_2O_3 and TiO_2 Grown by atomic layer deposition*, Chem. Vap. Depos. (2014), https://doi.org/10.1002/cvde.201407113.
[11] B.M. van der Ende, L. Aarts, A. Meijerink, Near-Infrared quantum cutting for photovoltaics, Adv. Mater. 21 (30) (2009) 3073–3077, https://doi.org/10.1002/adma.200802220.
[12] P. Boutinaud, et al., Quenching of lanthanide emission by intervalence charge transfer in crystals containing closed shell transition metal ions, Spectrosc. Lett. 40 (2) (2007) 209–220, https://doi.org/10.1080/00387010701247019.
[13] P.-A. Hansen, et al., Luminescence properties of lanthanide and ytterbium lanthanide titanate thin films grown by atomic layer deposition, J. Vac. Sci. Technol.: Vac. Surf. Films 34 (1) (2016), 01A130, https://doi.org/10.1116/1.4936389.
[14] M. Getz, et al., *Luminescent $YbVO_4$ by atomic layer deposition*, Dalton Trans. 46 (9) (2017) 3008–3013, https://doi.org/10.1039/C7DT00253J.
[15] M.N. Getz, et al., *Intense NIR emission in YVO_4: Yb^{3+} thin films by atomic layer deposition*, J. Mater. Chem. C (2017), https://doi.org/10.1039/C7TC02135F.
[16] Qu, M., et al., *Broadband near infrared quantum cutting in Bi – Yb codoped Y_2O_3 transparent films on crystalline silicon.* J. Lumin., (0). DOI: 10.1016/j.jlumin.2011.12.068.
[17] P. Gerner, H.U. Güdel, *Absorption and upconversion light emission properties of Er^{3+} and Yb^{3+}/Er^{3+} codoped $NaYS_2$*, Chem. Phys. Lett. 413 (1–3) (2005) 105–109, https://doi.org/10.1016/j.cplett.2005.07.072.
[18] V. Jarý, et al., *$ALnS_2$:RE (A=K, Rb; Ln=La, Gd, Lu, Y): New optical materials family*, J. Lumin. 170 (2016) 718–735, https://doi.org/10.1016/j.jlumin.2015.08.080.
[19] V. Jarý, et al., *Optical properties of Ce^{3+}-doped $KLuS_2$ phosphor*, J. Lumin. 147 (2014) 196–201, https://doi.org/10.1016/j.jlumin.2013.11.013, 0.
[20] A. Garcia, F. Guillen, C. Fouassier, *Charge transfer excitation of the Nd^{3+}, Sm^{3+}, Dy^{3+}, Ho^{3+}, Er^{3+} and Tm^{3+} emission in $CaGa_2S_4$*, J. Lumin. 33 (1) (1985) 15–27, https://doi.org/10.1016/0022-2313(85)90025-0.
[21] J. Šulc, et al., *Infrared spectroscopic properties of low-phonon lanthanide-doped $KLuS_2$ crystals*, J. Lumin. 211 (2019) 100–107, https://doi.org/10.1016/j.jlumin.2019.03.005.
[22] J. Zhang, et al., *Near-infrared luminescence characteristics of Yb^{3+}- and Er^{3+}-codoped $NaYS_2$ powder material*, J. Lumin. 152 (2014) 145–147, https://doi.org/10.1016/j.jlumin.2013.12.002.
[23] Y. Wang, et al., Physical manipulation of lanthanide-activated photoluminescence, Ann. Phys. 531 (9) (2019) 1900026, https://doi.org/10.1002/andp.201900026.
[24] G. Du, et al., *The influence of high magnetic field on electric-dipole emission spectra of Eu^{3+} in different single crystals*, J. Mater. Chem. C 1 (45) (2013) 7608–7613, https://doi.org/10.1039/C3TC31385A.
[25] F.L.M. Bernal, et al., *The Jahn-Teller Active Fluoroperovskites $ACrF_3$ A=Na^+,K^+: Thermo- and Magneto Optical Correlations as Function of the A-Site*, 2020 arXiv: 2005.06212 [cond-mat.mtrl-sci].
[26] G.H. Dieke, H.M. Crosswhite, H. Crosswhite, Spectra and Energy Levels of Rare Earth Ions in Crystals, Interscience Publishers, 1968.
[27] L. Aarts, et al., *Downconversion for solar Cells in $YF_3:Pr^{3+}$, Yb^{3+}*, Spectrosc. Lett. 43 (5) (2010) 373–381, https://doi.org/10.1080/00387010.2010.486731.
[28] R. Valiente, et al., *Er^{3+} luminescence as a sensor of high pressure and strong external magnetic fields*, High Pres. Res. 29 (4) (2009) 748–753, https://doi.org/10.1080/08957950903371716.